

Stage I lung adenocarcinoma: the value of quantitative CT in differentiating pathological subtypes and predicting growth of subsolid nodules

Xianqun Xu, MD^{a,*}, Kaisong Wu, MD, PhD^b, Yanyan Zhao, MD^b, Liejun Mei, MD, PhD^c

Abstract

The aim of this study was to investigate feasibility of quantitative computed tomography (CT) measurements in predicting invasiveness and growth of nodular ground glass opacities (nGGOs).

A set of 203 patients (group A) with nGGOs that were confirmed stage-I adenocarcinomas and 79 patients (group B) with nGGOs that were completely followed up were included. Lesions diameters, volume (VOL), maximum (MAX), mean (MEN), and standard deviation (STD) of CT attenuation were measured. P53 labeling index (LI) was evaluated through immunohistochemistry in group-A patients. Multivariate linear stepwise regressions were performed based on group-A lesions to calculate P53-LI prediction from CT measurements. The receiver operating characteristic (ROC) curve analyses were performed to assess the performance of P53-LI prediction in predicting invasiveness and growth of nGGOs. The Cox regression analysis was conducted to identify correlation between P53-LI Prediction and volume doubling time (VDT) of lesions in group B.

Diameter, VOL, MEN, STD, and the P53 LI showed significant differences between lesions of different pathological invasiveness ($P < .01$). By multivariate linear regressions, MEN and STD were identified as independent variables indicating P53 LI ($P < .001$); thus, an equation was established to calculate P53-LI Prediction as: $P53_{LI} Prediction = 0.013 \times MEN + 0.024 \times STD + 9.741$ (R square = 0.411, $P < .001$). The P53-LI Prediction showed good performance, similar as the actual one, in differentiating pathological invasiveness of nGGOs. In addition, the P53-LI Prediction demonstrated excellent performance in predicting growth of nGGOs (AUC = 0.833, $P < .001$) and independently forecasted VDT of nGGOs ($\beta = 1.773$, $P < .001$).

The P53-LI Prediction that was calculated from preoperative quantitative CT measurements of nGGOs indicates lesions' invasiveness and allows for predicting growth of nGGOs.

Abbreviations: AIS = adenocarcinoma in situ, CT = computed tomography, INV = nonlepidic-predominant adenocarcinoma, LI = labeling index, LPA = lepidic-predominant adenocarcinoma, MAX = maximum CT attenuation, MEN = mean CT attenuation, MIA = minimally invasive adenocarcinoma, nGGOs = nodular ground glass opacities, STD = standard deviation of CT attenuation, VDT = volume doubling time, VOL = volume.

Keywords: adenocarcinoma, ground glass opacity, high-resolution computed tomography, lung cancer, P53

1. Introduction

Subsolid nodules, also known as nodular ground glass opacities (nGGOs), are challenging, given their poorly defined margins, heterogeneous internal features, and varying attenuations.^[1,2] Pathologies of nGGOs are commonly associated with lung

adenocarcinomas, whose classification were recently revised by the International Association for the Study of Lung Cancer (IASLC)/American Thoracic Society (ATS)/European Respiratory Society (ERS), aiming to provide more specific diagnosis and better stratification.^[3-6] Pathologic differentiations of nGGOs have been imperative and attractive for thoracic surgeons, as different subtypes necessitate different treatments and will present with distinctive prognosis.^[5,6]

The *p53* suppressor gene plays a critical role in tumor genesis and progression. Immunohistochemical assessment of mutant P53 has been commonly used in clinical diagnosis and prognosis of lung cancer.^[7-9] However, the P53 labeling can only be obtained invasively either from operation or from biopsy. The evaluation of nGGOs may benefit particularly from computed tomography (CT), which has contributed to an increased detection of lung cancer at earlier and more curable stages.^[10] Many CT characteristics of nGGOs have been proposed for differentiating benign or indolent nGGO from malignant and invasive one, such as the diameter, volume, mass, attenuation, and heterogeneity, etc.^[11-13] Understanding the correlation between quantitative CT parameters and histologies of nGGOs may enable noninvasive characterization of suspected primary lung adenocarcinoma and may aid in decision as to whether lung

Editor: Mariusz Adamek.

The authors declare that there is no conflict of interest regarding this article.

^a Department of Clinical Laboratory, ^b Department of Respiration, ^c Department of Radiology, Zhongnan Hospital of Wuhan University, Wuhan, China.

* Correspondence: Xianqun Xu, Department of Clinical Laboratory, Zhongnan Hospital of Wuhan University, No. 169 in Donghu Road, Wuhan 430071, Hubei Province, P.R. China (e-mail: leometeor0422@hotmail.com).

Copyright © 2017 the Author(s). Published by Wolters Kluwer Health, Inc. This is an open access article distributed under the terms of the Creative Commons Attribution-Non Commercial-No Derivatives License 4.0 (CCBY-NC-ND), where it is permissible to download and share the work provided it is properly cited. The work cannot be changed in any way or used commercially without permission from the journal.

Medicine (2017) 96:16(e6595)

Received: 26 October 2016 / Received in final form: 18 March 2017 / Accepted: 22 March 2017

<http://dx.doi.org/10.1097/MD.0000000000006595>

resection is undertaken. Therefore, it is important to obtain an index that reflects both radiological and pathological characteristics of invasive nGGOs, in order to identify optimal target population.

In this study, we first established a prediction model incorporating parameters from CT image with immunohistochemical P53 labeling for assessing pathological invasiveness of nGGOs based on a set of patients who had experienced operations. Then, we tested the prognostic value of this model in another set of GGO patients who had been followed up for 5 years.

2. Methods

2.1. Patient selection

This study was approved by the Institutional Research Board. Informed consents were obtained from all patients included.

First, for establishing prediction model of P53 labeling index (LI), we retrospectively selected 203 patients (group A) with single nGGO who were resected and pathologically confirmed stage-I adenocarcinomas between January 01, 2010, and May 30, 2016, from the lung cancer registration system of our hospital. Chest high-resolution CT (HRCT) images that were closest to the date of tumor resection were retrieved. Of the 203 patients, 74 were men and 102 were women. The mean age of entire cohort was 52.1 ± 7.2 years (standard deviation, SD). The mean interval between the date of the closest preoperative HRCT study and the date of operation was 13.7 ± 6.2 days.

Then, we enrolled another set of 79 patients (group B) with single nGGO who did not experience operation but were consequentially followed up for 5 years to test the prediction model. We closed the follow-up work when patient met anyone of the following: 1) lesion's volume doubled, 2) death or imperative operation was done, 3) came to the end of study, 4) lost to follow -p. Follow-up CT examinations were reviewed.

2.2. Chest CT acquisition and nodule analysis

All chest CT images were obtained with a 16-detector-row (Somatom Sensation 16; Siemens, Forchheim, Germany) CT scanner using the following parameters: 120kV, 100mA, collimation of 16×0.75 mm, beam pitch of 0.7, and gantry rotation time of 0.5 s. Raw data were reconstructed for HRCT with thickness of 1 mm, interval of 0.75 mm, and a bone algorithm for reconstruction of lung.

After a training session of 5 cases, a radiological resident and a 12th-year postgraduate radiological student independently performed measurements of nGGOs, blinding to the pathological diagnosis. According to established method,^[14] a series of regions of interests (ROIs) delineating nodule outlines on all transverse images covering as large an area as possible from the whole lesion but excluding any blood vessels or chest wall abutting nodular margin were drawn electronically (manually adjusted if necessitated). Then, the computer automatically calculated volume (VOL) through multiplying the number of voxels by the unit volume of a voxel, as well as the diameter, maximum (MAX), mean (MEN), and standard deviation (STD) of CT attenuations of the total nGGO. The diameter was the maximal dimension on axial images.

For the follow-up evaluation, only diameter, VOL, and MEN were measured. Lesions were classified as stable or growing, with growth being defined as attenuation increases of at least 30 HU and (or) diameter increases by at least 20% in nodule of ≥ 10 mm,

or at least 30% in nodules of 5 to 9 mm.^[15,16] For growing nGGO, the volume doubling time (VDT), when happened, was recorded in unit of month.

2.3. Pathological diagnosis and P53-LI evaluation of lesions in group-A patients

According to the newly introduced IASLC/ATS/ERS classification,^[5] lesions' pathological sections of group-A patients were reviewed by a pulmonary pathologist with more than 5 years of experience, blinding to imaging findings. First, the specimens were categorized as adenocarcinoma in situ (AIS), minimally invasive adenocarcinoma (MIA), lepidic-predominant adenocarcinoma (LPA), acinar, papillary/micropapillary, solid, and invasive adenocarcinoma. Then, AIS and MIA (AIS/MIA) were grouped together, while LPA, acinar, papillary/micropapillary, and solid histologic subtypes that had relatively high-grade patterns of invasion compared with AIS/MIA were grouped together as LPA for analysis. The invasive subtypes were considered as 1 group of invasive nonlepidic-predominant adenocarcinoma (INV).

Then, immunostaining with the antibody for P53 was performed on specimens of group-A patients according to established methodology.^[17] The P53-positive nucleus were stained brown. An Olympus BX 50 microscope equipped with a cannon camera (Olympus, Tokyo, Japan) was used for microscopy and image capturing. Percentage of positive cells was quantitatively calculated by using Image Pro Plus 6.0 (Media Cybernetics, Washington, DC; Fig. 1), which has been widely used in biomedicine.^[17-19]

2.4. Statistical analysis

The intraclass correlation coefficients (ICCs) were calculated for analyzing interobserver agreements between the 2 observers, with values greater than 0.75 indicating good agreement.^[20] All statistical analyses were performed using SPSS 20 (IBM SPSS Inc., Chicago, IL) based on mean values of each measurement obtained by the 2 observers, with a 2-sided *P* value of $< .05$ indicating statistical significance. Intergroup differences were analyzed by using the 1-way analysis of variance (ANOVA) with post-hoc test being performed by using the Kruskal-Wallis test. To establish equation for calculating P53-LI Prediction, multivariate stepwise linear regressions were conducted. Then, the P53-LI Prediction was compared with actual P53-LI in relation to their capacities in predicting invasiveness and growth of nGGOs by using receiver operating characteristic curve (ROC) analyses. On the basis of data of group-B patients, the multivariate Cox regression was conducted to identify independent variables that could predict lesions' VDT.

3. Results

3.1. Basic, pathological information, and nodule measurements of group-A patients

Pathologically, 81 lesions were diagnosed as AIS/MIA, while 78 and 44 lesions were, respectively, LEP and INV, in group-A patients. The differences of gender and age distributions among the pathological subtypes of nGGOs were not significant ($P > .05$, Table 1).

The interobserver agreements were excellent for automated measurements between the 2 observers with the ICC ranging from 0.811 to 0.912. All CT parameters of nGGOs showed

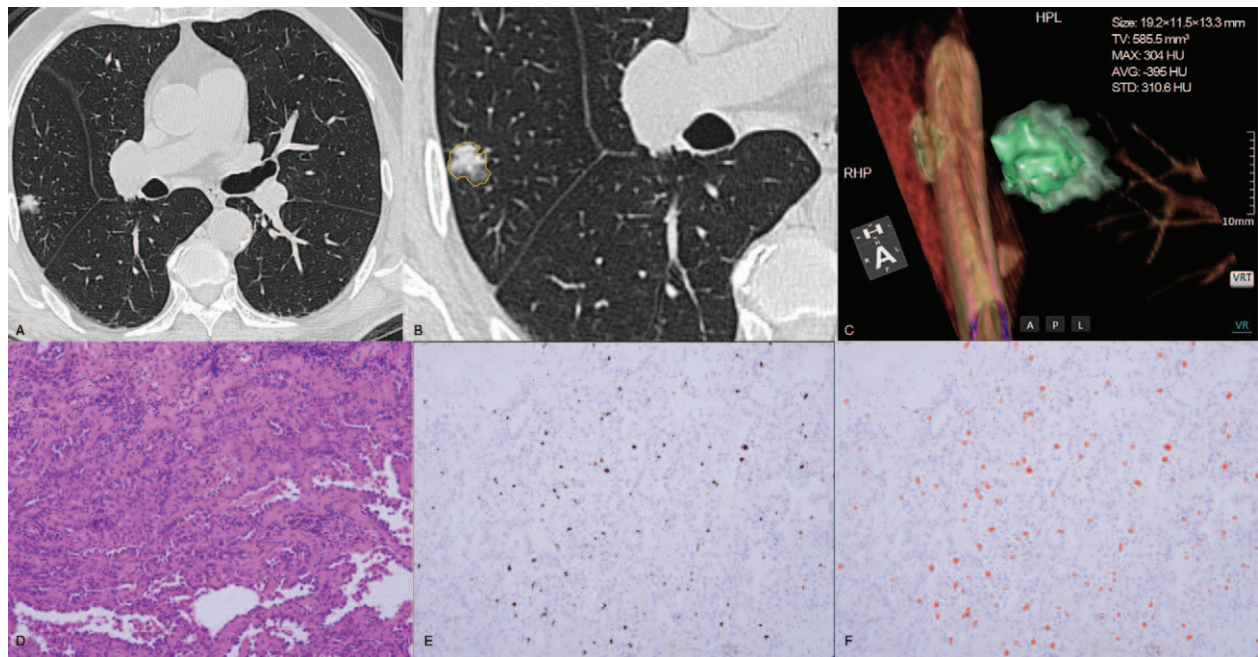


Figure 1. Evaluation of a GGO nodule by quantitative CT and P53 immunohistochemistry. (A) Representative transversal image of chest high resolution CT (HRCT) shows that the nodule is located in the right upper lobe of lung. (B) Transversal HRCT with a zoom ratio of 2.0 presents outline delineation of the nodule. (C) Image of volume render technique (VRT) shows the overlay and measurements of the entire nodule. (D) Pathological image of Hematoxylin-Eosin staining (magnification, $\times 100$) confirms that the nodule is invasive adenocarcinoma, postoperatively. (E) Immunohistochemical image of P53 staining (magnification, $\times 100$) with nucleus of tumor cells that are positive for P53 being stained as tan particles. (F) Quantitative measurement of the P53 labeling index by Image Pro Plus 6.0 (red areas denote detection of the software).

significant differences among pathological subtypes ($P < .01$), except MAX, which failed to differentiate INV from LEP ($P2 = .087$; Table 1).

3.2. Correlations between P53 LI and nodule measurements on CT

The multivariate linear stepwise regressions identified that MEN and STD were independent variables predicting P53 LI (P values all $< .001$), with STD having the largest standardized

β -coefficient (0.381) indicating the largest power in predicting P53 LI, as summarized in Table 2. However, diameter, VOL, and MAX (P values all $> .05$) were excluded from the final model of the stepwise regressions, which means that they were not independent factors predicting P53 LI. Consequently, an equation for calculating P53-LI Prediction was established as follows:

$$\text{P53LI Prediction} = 0.013 \times \text{MEN} + 0.024 \times \text{STD} + 9.741$$

R square = 0.411, $P < .01$.

Table 1
Demography, CT measurements, and pathologies of nGGOs from group-A patients (n=203).

Variables	AIS/MIA	LEP	INV	P	P1	P2	ICC
Gender				.258	NA	NA	NA
Male	40	34	15				
Female	41	44	29				
Age, y	51.0 \pm 8.6	53.1 \pm 8.2	51.8 \pm 7.6	.267	NA	NA	NA
CT measurements							
Diameter, mm	13.1 \pm 4.8	16.0 \pm 6.3	21.0 \pm 6.3	$< .001$.004	$< .001$	0.841
VOL, mm ³	661.7 \pm 394.7	1078.8 \pm 607.1	1635.6 \pm 948.3	$< .001$	$< .001$.002	0.862
MAX, HU	-79.8 \pm 200.0	60.1 \pm 172.8	177.8 \pm 325.7	$< .001$	$< .001$.087	0.811
MEN	-464.0 \pm 41.5	-427.7 \pm 40.7	-401.9 \pm 44.3	$< .001$	$< .001$.001	0.877
STD	112.2 \pm 30.6	153.1 \pm 36.5	181.8 \pm 33.4	$< .001$	$< .001$	$< .001$	0.912
P53 LI (%)	5.4 \pm 2.0	8.0 \pm 1.9	10.5 \pm 1.6	$< .001$	$< .001$	$< .001$	NA
P53 LI Prediction (%)	6.1 \pm 1.0	7.6 \pm 0.9	8.7 \pm 1.2	$< .001$	$< .001$	$< .001$	NA

Unless otherwise indicated, numerical variables were recorded as mean \pm standard deviation. Age, MEN, STD, P53 LI, and P53 LI Prediction were analyzed by 1-way ANOVA analysis and least significant difference (LSD) test. Diameter, VOL, and MAX were analyzed by Kruskal–Wallis and Tamhane T2 test. P indicates the P values for 1-way ANOVA or Kruskal–Wallis analyses of all nGGOs; $P1$ indicates the P values for LSD test or Tamhane T2 test of AIS/MIA vs LEP; $P2$ indicates the P values for LSD test or Tamhane T2 test of LEP vs INV.

AIS=adenocarcinoma in situ, HU=Hounsfield unit, ICC=intraclass coefficients, INV=invasive adenocarcinoma, LEP=lepidic-predominant adenocarcinoma, LI=labeling index, MAX, MEN and STD denotes maximum, mean, and standard deviation of CT attenuation within ground-glass-opacity nodules, MIA=minimally invasive adenocarcinoma, NA=not associated, VOL=volume.

Table 2
Multivariate stepwise linear regression analysis (dependent variable: P53 LI).

Variables	Unstandardized β -coefficients	SE	Standardized β -coefficients	P
MEN	0.013	0.004	0.231	<.001
STD	0.024	0.004	0.381	<.001
Constant	9.741	1.878	NA	<.001

Diameter, VOL (volume), and MAX (maximum CT attenuation) were excluded from the final regression model. MEN = mean CT attenuation, NA, not associated, SE = standard error, STD = standard deviation of CT attenuation.

The P53-LI Prediction was calculated as 6.1 ± 1.0 for AIS/MIA lesions, 7.6 ± 0.9 for LEP lesions, and 10.5 ± 1.6 for INV lesions with significant intergroup differences ($P < .001$; Table 1). Furthermore, we compared the diagnostic performance of P53-LI Prediction with the actual one by comparing their AUCs (Fig. 2). The P53-LI Prediction showed a little higher AUCs than the actual P53 LI either in differentiating LEP from AIS/MIA (AUC 0.870 vs 0.831, $P = .361$; Fig. 2A) or in differentiating INV from LEP (AUC 0.846 vs 0.762, $P = .127$; Fig. 2B), although not statistically significant. The optimal thresholds of P53-LI Prediction for differentiating LEPs from AIS/MIAs and for differentiating INVs from LEPs were 6.6% and 8.0%, respectively, with corresponding sensitivity being 87.2% and 81.8%, and specificity being 72.8% and 75.6%, respectively (Fig. 2).

3.3. Follow-up, demography, and nodule evaluation of patients in group B

In patients from group B, 38 (55.1%) were male and 31 (44.9%) were female, with age being 51.9 ± 7.99 years (mean \pm SD). There was no significant difference in sex ratio or age distribution between stable and growing lesions ($P = .689$ and $.063$, respectively; Table 3). During follow-up, 8 (10.1%) cases were censored because of imperative operation ($n = 3$), lost in follow-up ($n = 2$), and death ($n = 3$). Finally, 61 patients were successfully

followed up, with a follow-up rate of 89.9%. Twenty nGGOs (29.0%) were stable during the 5-year period, while 49 (71.0%) lesions showed a growing pattern. Of the 49 patients with growing nGGOs, 7 cases were closed to follow-up before the end of the 5-year period because of imperative operation ($n = 5$) and death ($n = 2$). Three cases failed to determine VDT. Eventually, 39 nGGOs presented with doubling volumes during the period of follow-up, with VDT being 27.6 ± 19.37 (Table 3).

The growing lesions showed significantly larger initial VOL, MAX, MEN, and STD than the stable ones ($P < .05$), while initial diameter was not significantly different between stable and growing lesions ($P = .102$, Table 3). On the basis of the equation established above, the P53-LI Prediction calculated were significantly higher in growing lesions than in stable lesions ($P < .001$, Table 3). The ROC analysis showed that the AUCs of lesions' initial diameter, VOL, MAX, MEN, STD, and P53-LI Prediction were 0.612, 0.666, 0.690, 0.753, 0.729, and 0.833, respectively, in predicting lesions growth. Obviously, the P53-LI Prediction owned the best prediction performance.

In addition, we performed stepwise Cox regression analysis to identify relationships between initial CT measurements of nGGOs and their VDT obtained during the follow-up period. Results are summarized in Table 4. Only Ki67-PI Prediction was an independent variable that could forecast VDT of growing nGGOs ($\beta = 1.773$, $P < .001$). In lesions with similar characteristics with respect to the variables analyzed, a 1% increase of P53-LI Prediction forecasts a 5.888-fold increase of probability that nGGOs will double in volume within 5 years.

4. Discussion

In this investigation, the quantitative CT measurements of subsolid nodular lung adenocarcinoma discriminated 3 cohorts of IASLC/ATS/ERS-classified lesions, and were significantly correlated with the postoperative immunohistochemical P53 LI. Furthermore, calculated from these CT measurements, the P53 LI Prediction even showed a slightly higher diagnostic performance, although not statistically significant, than the actual P53 LI in differentiating pathological subtypes of nGGOs

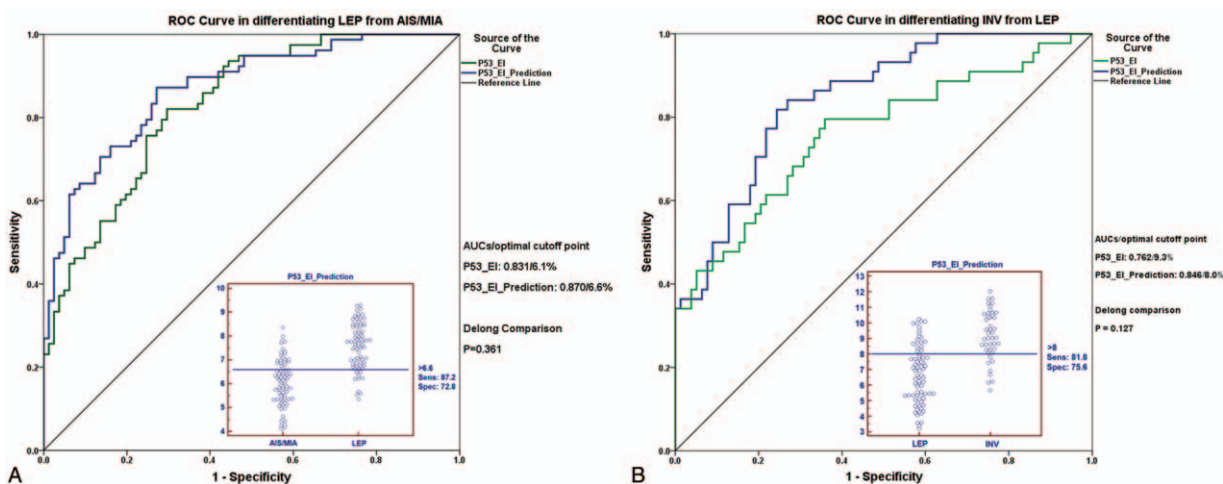


Figure 2. The receiver operating characteristic curve (ROC) analyses of P53-LI Prediction and the actual P53 LI in differentiating LEP from AIS/MIA (A) and in distinguishing INV from LEP (B). Areas under the curve (AUCs) of P53-LI Prediction are higher than the actual P53 LI (although not statistically significant) either in differentiating LEP from AIS/MIA (AUC 0.870 vs 0.831, $P = .361$) or in distinguishing INV from LEP (AUC 0.846 vs 0.762, $P = .127$) according to the method described by Delong et al. Inserted are interactive dot diagrams showing optimal cutoffs of P53-LI Prediction in differentiating LEP from AIS/MIA (A) and in distinguishing INV from LEP (B), with corresponding sensitivity being 87.2% and 81.8%, respectively, and specificity being 72.8% and 75.6%, respectively.

Table 3
Demographic, radiological, and follow-up information of nGGOs from group-B patients (n=69).

Variables	Stable	Growing	P
Gender			.689*
Male	19	19	
Female	14	17	
Age, y	49.5±8.63	53.2±6.95	.063†
Initial CT measurements			
Diameter, mm	14.0±6.81	16.9±6.66	.102†
VOL, mm ³	714.4±616.81	1184.3±740.71	.015†
MAX, HU	-103.8±194.52	90.7±215.87	.001†
MEN	-471.0±35.58	-424.9±42.14	<.001†
STD	111.6±42.79	156.6±40.91	<.001†
P53 LI Prediction (%)	5.9±1.12	7.8±1.29	<.001†
Volume-doubled lesions	0	39	
Doubling time, mo	NA	27.6±19.37	

Unless otherwise indicated, numerical variables were recorded as mean±standard deviation. HU=Hounsfield unit, LI=labeling index, MAX, MEN and STD denotes maximum, mean, and standard deviation of CT attenuation within ground-glass opacity nodules, respectively, NA = not associated, VOL = volume.
* Chi-square test.
† Student t test.

and presented as an excellent predictor in forecasting the growth of nGGOs.

The findings in the present study have great significance. As the multidisciplinary IASLC/ATS/ERS classification system was issued in 2011 in response to the need to better classify lesions and differentiate patients with varying survivals, pathological differentiation of nGGOs has been imperative and attractive for thoracic surgeons.^[5,21,22] AIS comprises only lepidic noninvasive growth. MIA and LPA are also predominantly lepidic but have invasive foci, which is less than 5 mm for MIA and larger than 5 mm for LPA.^[5] AIS, MIA, and LPA have 5-year disease-free survival rates of 100%, near 100%, and 90%, respectively.^[5,22] The 5-year disease-free survival rates of acinar- and papillary-predominant forms have been reported to be 84% and 83%, respectively, while those of micropapillary-and solid-predominant adenocarcinomas have been reported to be 67% and 70%, respectively.^[5] Therefore, it is necessary to develop a prediction model that can differentiate malignant or invasive nGGO from benign one in order to identify optimal target population for treatment.

In recent years, advances in imaging technology have promoted a more precise and quantitative pattern in assessing nGGOs than traditional 1-dimensional or 2-dimensional methods.^[11,13,23] In patients with nGGOs at lung cancer screening, de Hoop et al^[24] reported intra- and interobserver coefficients of variation (15% and 18%, respectively) for volumes that were derived from manually acquired linear 2-dimensional measures to be greater than those from manually segmented 3D mass (9%)

Table 4
Multivariate stepwise Cox regression analysis (dependent variable: Doubling time).

Variables	β-coefficients	SE	Wald	HR [exp (β)]	P
P53 LI Prediction	1.773	0.268	43.718	5.888	<.001

Diameters, VOL (volume), MEN (mean CT attenuation), MAX (maximum CT attenuation), and STD (standard deviation of CT attenuation) were excluded from final regression model. HR = hazard ratio, SE = standard error.

or volumes.^[25] Visual assessment had only moderate agreement when determining nodule attenuation; identifying the presence of or amount of solid component was the major cause of variation.^[26] Therefore, the quantitative method may be more suitable for assessing nGGOs given their continuous progression, pathologically, that advance from AIS/MIA through LEP and finally to INV. For instance, pre-invasive nGGOs (including AIS/MIA) most likely own a low MAX, MEN, and STD, while invasive lesions (including LEP and INV) generally own higher MAX, MEN, and STD, and commonly present as mix GGOs or come up to be solid nodes with increased diameters and VOL.^[6,17,27] It is reasonable to associate quantitative CT measurements with histopathologies of nGGOs for improved preoperative differentiation of invasiveness of subsolid nodules.

The p53 gene is well known regarding its anticancer function.^[28,29] It has been reported that the solid component of a nGGO was significantly associated with expression of mutant P53 protein within tumor, indicating invasive growth and poor prognosis.^[12,30] In the present study, the immunohistochemical index—P53 LI—showed good diagnostic performance in differentiating nGGOs of different invasiveness. Furthermore, the MEN and STD were identified as independent parameters indicating P53 LI of nGGOs (P<.001, Table 3). Calculated from these 2 measurements of nGGOs, the P53-LI Prediction of nGGOs showed similar capacity as the actual P53 LI in differentiating nGGOs of different invasiveness. In addition, the P53-LI Prediction presented as a good predictor in indicating the growth of nGGOs. The MEN describes nGGO in terms of its substantiality, while STD reflects its tissue heterogeneity. Therefore, we consider that the proposed regression model and equation in this study for calculating P53-LI Prediction are reasonable and valuable.

Nodular GGOs comprise a variety of pathologies with only about 34% of lesions were reported to be malignancies; some of the malignant lesions even showed an indolent growing pattern.^[31] It has been reported that approximately 52% of the GGO lesions presented with a slow rate of growth (<2mm per year).^[32] In this study, a similar percentage (47.8%, 33/69) of the total followed-up nGGOs were stable during the 5-year period. Even for the growing nGGOs, their VDTs were not short (27.6±19.37 months). Thus, it is important to differentiate benign and indolent nGGO from malignant and invasive one before operation, in order to avoid unnecessary surgery. Interestingly, the calculated P53-LI Prediction in this study based on initial CT measurements demonstrated excellent performance in differentiating growing nGGOs from stable ones. In addition, the P53-LI Prediction also independently predicted the VDT of the growing nGGOs. This noninvasive index may be of great importance to the treatment selection and the prognosis evaluation of a specific GGO node.

Several limitations of this study should be mentioned. First, the P53-LI Prediction was a virtual index that was calculated from MEN and STD of nGGOs. Therefore, its practicability needs to be confirmed. Second, we just established a prediction model from data of patients from group A, while tested it in another set of patients (group B). Thus, the result of this study might have suffered from impact of inter-patient variations. Researches that are performed with only 1 set of patients who have been fully followed-up to surgeries for establishing and testing the prediction model within only 1 patient group are needed. Third, this study was performed in a single institution with limited case sample. Thus, the result should only be explained within this study.

In conclusion, the P53-LI Prediction that was calculated from preoperative quantitative CT measurements of nGGOs indicates lesion invasiveness and allows for predicting growth of nGGOs.

References

[1] Hansell DM, Bankier AA, MacMahon H, et al. Fleischner Society: glossary of terms for thoracic imaging. *Radiology* 2008;246:697–722.

[2] Ko JP, Suh J, Ibdapo O, et al. Lung adenocarcinoma: correlation of quantitative CT findings with pathologic findings. *Radiology* 2016;280:931–9.

[3] Saito H, Yamada K, Hamanaka N, et al. Initial findings and progression of lung adenocarcinoma on serial computed tomography scans. *J Comput Assist Tomogr* 2009;33:42–8.

[4] Sumikawa H, Johkoh T, Nagareda T, et al. Pulmonary adenocarcinomas with ground-glass attenuation on thin-section CT: quantification by three-dimensional image analyzing method. *Eur J Radiol* 2008;65:104–11.

[5] Travis W, Brambilla E, Noguchi M, et al. International association for the study of lung cancer/American Thoracic Society/European Respiratory Society international multidisciplinary classification of lung adenocarcinoma. *J Thorac Oncol* 2011;6:244–85.

[6] Lee HY, Choi YL, Lee KS, et al. Pure ground-glass opacity neoplastic lung nodules: histopathology, imaging, and management. *AJR Am J Roentgenol* 2014;202:W224–33.

[7] Aoki T, Hanamiya M, Uramoto H, et al. Adenocarcinomas with predominant ground-glass opacity: correlation of morphology and molecular biomarkers. *Radiology* 2012;264:590–6.

[8] Ciancio N, Galasso MG, Campisi R, et al. Prognostic value of p53 and Ki67 expression in fiberoptic bronchial biopsies of patients with non small cell lung cancer. *Multidiscip Respir Med* 2012;7:1–6.

[9] Yamaguchi F, Kugawa S, Tateno H, et al. Analysis of EGFR, KRAS and P53 mutations in lung cancer using cells in the curette lavage fluid obtained by bronchoscopy. *Lung Cancer* 2012;78:201–6.

[10] Aberle DR, Adams AM, Berg CD, et al. Reduced lung-cancer mortality with low-dose computed tomographic screening. *N Engl J Med* 2011;365:395–409.

[11] Tamura M, Shimizu Y, Yamamoto T, et al. Predictive value of one-dimensional mean computed tomography value of ground-glass opacity on high-resolution images for the possibility of future change. *J Thorac Oncol* 2014;9:469–72.

[12] Son JY, Lee HY, Lee KS, et al. Quantitative CT analysis of pulmonary ground-glass opacity nodules for the distinction of invasive adenocarcinoma from pre-invasive or minimally invasive adenocarcinoma. *PLoS One* 2014;9:e104066.

[13] Jin X, Zhao SH, Gao J, et al. CT characteristics and pathological implications of early stage (T1N0M0) lung adenocarcinoma with pure ground-glass opacity. *Eur Radiol* 2015;25:2532–40.

[14] Ko JP, Berman EJ, Kaur M, et al. Pulmonary nodules: growth rate assessment in patients by using serial CT and three-dimensional volumetry. *Radiology* 2012;262:662–71.

[15] Liang M, Liu X, Li W, et al. Evaluating the growth of pulmonary nodular ground-glass opacity on CT: comparison of volume rendering and thin slice images. *J Huazhong Univ Sci Technolog Med Sci* 2011;31:846–51.

[16] Sone S, Nakayama T, Honda T, et al. Long-term follow-up study of a population-based 1996–1998 mass screening programme for lung cancer using mobile low-dose spiral computed tomography. *Lung Cancer* 2007;58:329–41.

[17] Peng M, Peng F, Zhang C, et al. Preoperative prediction of Ki-67 labeling index by three-dimensional CT image parameters for differential diagnosis of ground-glass opacity (GGO). *PLoS One* 2015;10:e129206.

[18] Wang CJ, Zhou ZG, Holmqvist A, et al. Survivin expression quantified by Image Pro-Plus compared with visual assessment. *Appl Immunohistochem Mol Morphol* 2009;17:530–5.

[19] Francisco JS, Moraes HP, Dias EP. Evaluation of the Image-Pro Plus 4.5 software for automatic counting of labeled nuclei by PCNA immunohistochemistry. *Braz Oral Res* 2004;18:100–4.

[20] Busing KA, Kilian AK, Schaible T, et al. Reliability and validity of MR image lung volume measurement in fetuses with congenital diaphragmatic hernia and in vitro lung models. *Radiology* 2008;246:553–61.

[21] Yoshizawa A, Motoi N, Riely GJ, et al. Impact of proposed IASLC/ATS/ERS classification of lung adenocarcinoma: prognostic subgroups and implications for further revision of staging based on analysis of 514 stage I cases. *Mod Pathol* 2011;24:653–64.

[22] Yoshizawa A, Sumiyoshi S, Sonobe M, et al. Validation of the IASLC/ATS/ERS lung adenocarcinoma classification for prognosis and association with EGFR and KRAS gene mutations: analysis of 440 Japanese patients. *J Thorac Oncol* 2013;8:52–61.

[23] Kostis WJ, Yankelevitz DF, Reeves AP, et al. Small pulmonary nodules: reproducibility of three-dimensional volumetric measurement and estimation of time to follow-up CT. *Radiology* 2004;231:446–52.

[24] de Hoop B, Gietema H, van de Vorst S, et al. Pulmonary ground-glass nodules: increase in mass as an early indicator of growth. *Radiology* 2010;255:199–206.

[25] Kim HY, Shim YM, Lee KS, et al. Persistent pulmonary nodular ground-glass opacity at thin-section CT: histopathologic comparisons. *Radiology* 2007;245:267–75.

[26] van Riel SJ, Sanchez CI, Bankier AA, et al. Observer variability for classification of pulmonary nodules on low-dose CT images and its effect on nodule management. *Radiology* 2015;277:863–71.

[27] Takahashi M, Shigematsu Y, Ohta M, et al. Tumor invasiveness as defined by the newly proposed IASLC/ATS/ERS classification has prognostic significance for pathologic stage IA lung adenocarcinoma and can be predicted by radiologic parameters. *J Thorac Cardiovasc Surg* 2014;147:54–9.

[28] Toyooka S, Tsuda T, Gazdar AF. The TP53 gene, tobacco exposure, and lung cancer. *Hum Mutat* 2003;21:229–39.

[29] Roy-Chowdhuri S, Chow CW, Kane MK, et al. Optimizing the DNA yield for molecular analysis from cytologic preparations. *Cancer Cytopathol* 2016;124:254–60.

[30] Lee HY, Lee KS. Ground-glass opacity nodules: histopathology, imaging evaluation, and clinical implications. *J Thorac Imaging* 2011;26:106–18.

[31] Henschke CI, Yankelevitz DF, Mirtcheva R, et al. CT screening for lung cancer: frequency and significance of part-solid and nonsolid nodules. *AJR Am J Roentgenol* 2002;178:1053–7.

[32] Koo CW, Miller WT, Kucharczuk JC. Focal ground-glass opacities in non-small cell lung carcinoma resection patients. *Eur J Radiol* 2012;81:139–45.